Photoreduction of Water by using Modified CuInS$_2$ Electrodes

Shigeru Ikeda,*[a] Takayuki Nakamura,[a] Sun Min Lee,[a] Tetsuro Yagi,[a] Takashi Harada,[a] Tsutomu Minegishi,[b] and Michio Matsumura[a]

Polycrystalline CuInS$_2$ films were fabricated by sulfurization of electrodeposited Cu and In metallic precursor films. Structural analyses revealed that the CuInS$_2$ film formed compact agglomerates of crystallites with grain sizes of ca. 0.5–1.5 μm. Photoelectrochemical characterization revealed that the film was p-type with a flat band potential of 0.3–0.4 V (vs Ag/AgCl at pH 4), which is suitable for water reduction but cannot be for water oxidation. Upon loading Pt deposits, the film worked as a hydrogen (H$_2$) liberation electrode under cathodic polari-

zation. Moreover, by introduction of n-type thin layers such as CdS and ZnS on the CuInS$_2$ surface before the Pt loading, appreciable improvements of H$_2$ liberation efficiency were achieved: for the CdS modified sample, spectral response data showed incident photon to current efficiency as high as 20% at wavelengths ranging from ca. 500 to 750 nm. Appreciable H$_2$ evolution on this sample under potentials of power-producing regions was also confirmed.

Introduction

Hydrogen production from water using abundant solar light is now an important research subject in view of energy and environmental issues.[1] Photocatalytic overall water splitting using heterogeneous semiconductor powders has been studied extensively as a promising means for ideal H$_2$ production on a large scale.[2–5] Various semiconductor materials, including mixed oxides,[2a,c,3] nitrides,[4] and oxynitrides,[2b,5] have been shown to induce efficient water splitting reaction; quantum yields higher than 50% have been reported for some photocatalytic systems.[3e,g] Due to the limitation of their relatively wide band gaps, however, the present efficiency under sunlight radiation is not sufficient for practical applications.

Photoelectrochemical water splitting has become another attractive approach since the first report of a TiO$_2$ thin-film photoelectrode.[6] A variety of semiconductor electrodes and devices have been investigated.[7–10] To date, performances with conversion efficiency as high as 10% have been demonstrated for electrodes based on stacked III–V semiconductors prepared by metal–organic chemical vapor deposition (MOCVD).[9] However, these electrodes have limited corrosion resistance in aqueous electrolytes and are expensive for practical applications. On the other hand, the well-studied transition metal oxides are corrosion-resistant and inexpensive, but conversion efficiencies for these electrodes are not sufficiently high yet due to the lack of optical and photoelectrochemical properties required for realizing high photocurrents and H$_2$ evolution rates.

Chalcopyrite p-type semiconductors such as CuInSe$_2$, CuGaSe$_2$, CuInS$_2$, and their mixed crystals are used as absorber layers in thin-film solar cells.[11] Due to their high absorption coefficient, 1–2 μm thick layers are enough to absorb the most part of the incident solar radiation. A wide range of band gap values (1.0–2.4 eV) can be obtained by changing the In/Ga

and/or Se/S ratios. These specific properties are also attractive for the use of a photocathode for H$_2$ production. Although there have been a few reports in which photoelectrochemical properties of the series of chalcopyrite families for H$_2$ production were discussed,[12] there have been little work on efficient H$_2$ production.[12e,f] Therefore, in the present study, we attempted to fabricate a CuInS$_2$-based photocathode for efficient H$_2$ production. For this purpose, we first investigated the photoelectrochemical properties of a polycrystalline CuInS$_2$ film in an electrolyte solution containing Eu^{III} as an electron acceptor. We then investigated the H$_2$ evolution property in detail, focusing on the importance of surface modification to form a p-n junction.

Results and Discussion

Structure of CuInS$_2$ film

In this study, a CuInS$_2$ film was fabricated from electrochemically stacked layers of metallic Cu and In followed by sulfurization (see the Experimental Section). The composition ratio of Cu and In (Cu/In) in the metallic precursor was fixed at a Cu-rich composition (Cu/In = ca. 1.3–1.4) compared to the stoi-

[a] Prof. S. Ikeda, T. Nakamura, S. M. Lee, T. Yagi, Dr. T. Harada,
Prof. M. Matsumura
Research Center for Solar Energy Chemistry
Osaka University
1–3 Machikaneyama, Toyonaka 560–8531 (Japan)
Fax: (+81) 6 6850 6699
E-mail: sikeda@chem.es.osaka-u.ac.jp

[b] Dr. T. Minegishi
Department of Chemical System Engineering
The University of Tokyo
7-3-1 Hongo, Bunkyo-ku, Tokyo 113-8656 (Japan)

chiometric ratio of the final CuInS$_2$ film. It is known that a high Cu/In ratio is desirable for obtaining a CuInS$_2$ film with high crystallinity and large grain sizes, due to the crucial role of Cu$_x$S impurity phase(s) to accelerate the growth of CuInS$_2$ crystallites during the sulfurization process.[11a,d]

The stacked metallic precursor film obtained on a Mo/glass substrate showed good uniformity and adherence. After sulfurization, the semi-glossy film with a white color became non-reflective. A slightly bluish gray color of the resulting film suggests surface coverage of the Cu$_x$S components.[11a] As can be seen in Figure 1 a, the XRD pattern of the thus-obtained film
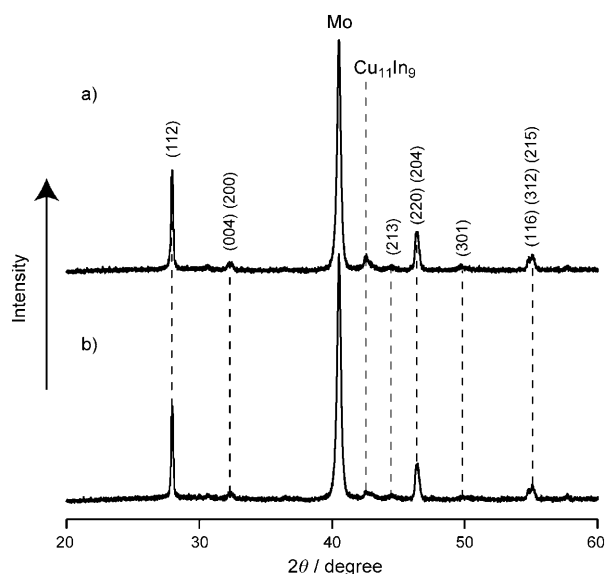

Figure 1. XRD patterns of CuInS$_2$ films a) before and b) after KCN etching.

showed typical diffraction peaks assignable to the CuInS$_2$ crystal with a chalcopyrite structure,[13] in addition to peaks due to the Mo substrate. The relatively high intensity of (112) reflection compared to that of (204) reflection indicates a high degree of preferred orientation of the CuInS$_2$ film towards the (112) direction. Since we took the Cu-rich composition for the synthesis of the CuInS$_2$ film, Cu$_x$S compounds should be present in the film; however, owning to their amorphous nature no diffraction peak can be assigned to these compounds. By KCN etching, these binary Cu compounds were dissolved out, as evidenced by the disappearance of the bluish color of the film, whereas no structural alteration of the CuInS$_2$ part occurred with this treatment (Figure 1 b). In addition, a weak peak derived from the Cu$_{11}$In$_9$ compound appeared at 2θ of ca. 43°[14] in both samples before and after KCN etching, indicating a slightly insufficient time or temperature of the present sulfurization treatment.

Figure 2 shows the scanning electron microscope (SEM) images of the CuInS$_2$ film after KCN etching. The top view SEM image indicates that the film consists of compact agglomerates of angular-shaped crystallites (Figure 2 a). A cross-sectional SEM image of the corresponding sample in Figure 2 b also shows regularly shaped crystals with grain sizes ranging from 0.5 to 1.5 µm. In addition, crevices were frequently observed at
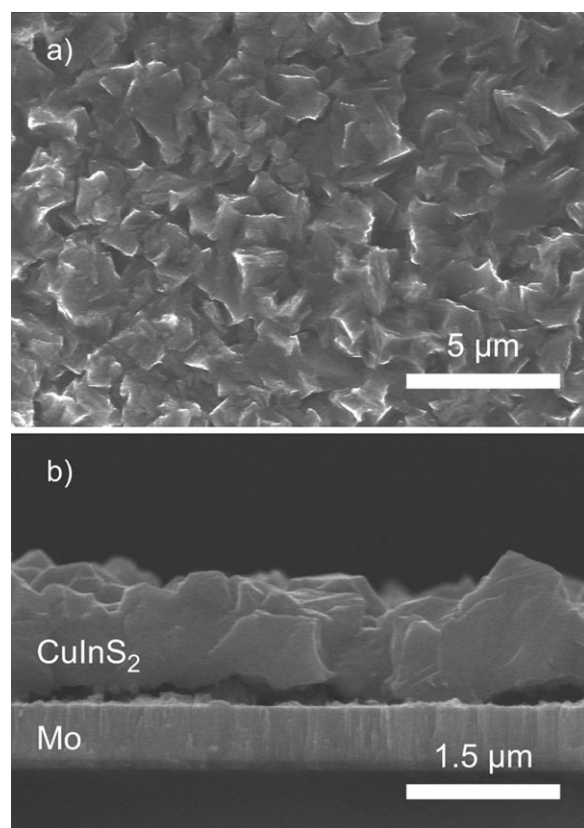

Figure 2. SEM images of the CuInS$_2$ film after KCN etching: a) top view and b) cross-sectional view.

the interface between the CuInS$_2$ crystallites and the top of the columnar Mo layer, probably due to peeling caused by sulfurization.

Photoelectrochemical properties of CuInS$_2$ film

The current–voltage characteristics of the CuInS$_2$ film were investigated by linear sweep voltammetry (LSV) in an aqueous Eu^{3+} solution, with pH adjusted to 4, at potentials from −0.55 to 0 (vs Ag/AgCl.). The potential sweep was performed in the anodic direction with a scan rate of 5 mV s^{-1} under chopped illumination from a 300 W xenon lamp. Figure 3 shows a typical LSV plot of the CuInS$_2$ film. As a cathodic photocurrent appeared, the CuInS$_2$ film prepared in the present study behaved as a *p*-type semiconductor electrode. The photocurrent increased as the electrode potential was made more negative; the photocurrent onset appeared at −0.05 V (vs Ag/AgCl). Assuming that the onset of the present *p*-type semiconductor occurred at potentials of ca. 0.2 V more negative than the flat band potential (V$_{fb}$), the V$_{fb}$ of CuInS$_2$ in the present electrolyte solution lies at ca. 0.15 V (vs Ag/AgCl).

Incident photon to current efficiency (IPCE) of the CuInS$_2$ electrode was measured under irradiation of monochromatic light with various wavelengths at −0.5 V vs Ag/AgCl. The obtained IPCE spectrum is shown in Figure 4 a. The onset region of the spectrum was analyzed to determine the band gap (E$_g$)
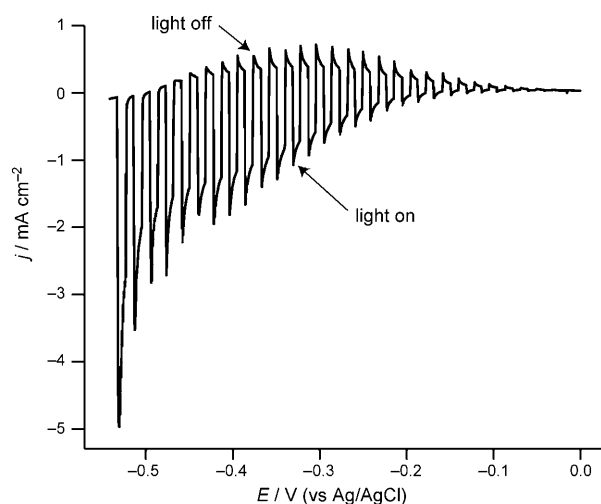
Figure 3. A linear sweep voltammogram of the CuInS$_2$ film in Eu^{III} nitrate (50 mmol L^{-1}) under chopped illumination from a Xe lamp.
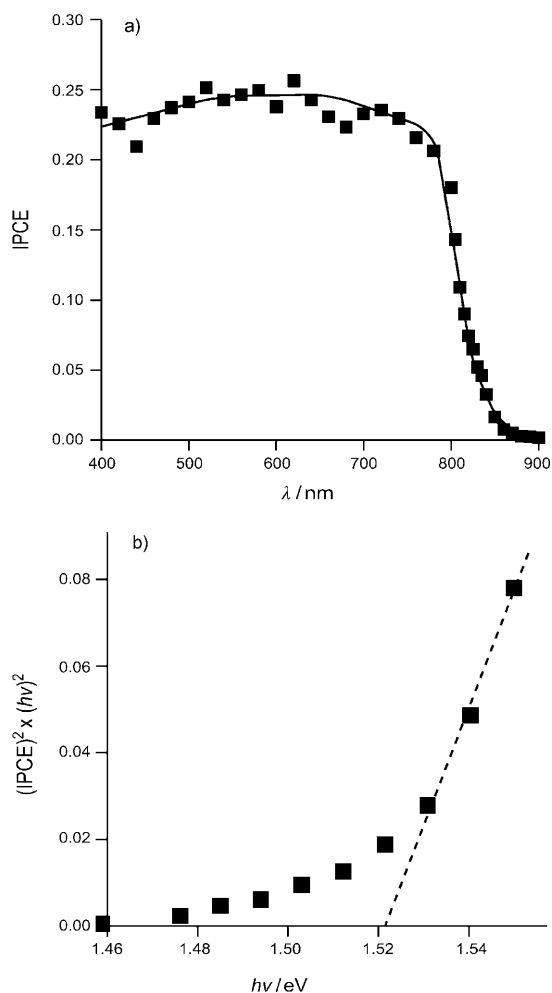

Figure 4. a) An incident photon to current efficiency of CuInS$_2$ measured at −0.5 V vs Ag/AgCl in Eu^{III} nitrate (50 mmol L^{-1}) under irradiation of monochromatic light with various wavelengths. b) Plots of (IPCE)^2×($h\nu$)^2 vs $h\nu$ for the CuInS$_2$ film. An intercept line denotes the E_g value.

of the present CuInS$_2$ electrode. As it has been reported previously,[15] IPCE can be related to E_g by the following equation:

$$(\text{IPCE}) \times (h\nu) = A(h\nu\text{-}E_g)^n \tag{1}$$

where $h\nu$ is the incident photon energy, A is a proportionality constant, and n varies from 0.5 to 2.0 depending on the nature of the optical transition. Because the transition is direct with CuInS$_2$, n of 0.5 is applied to them. Figure 4b shows the plot of (IPCE)^2×($h\nu$)^2 against $h\nu$ for the CuInS$_2$ electrode. Because a linear relation was obtained as predicted by Equation (1), E_g was determined from the intercept of the photon energy ($h\nu$) axis. The E_g value was determined to be ca. 1.52 eV, which is almost the same as the reported E_g value of 1.53 eV.[16]

Based on the above results, the conduction band edge (V_{CB}) and balance band edge (V_{VB}) were estimated to lie at −1.3 V and 0.2 V (vs Ag/AgCl), respectively. In the pH region, the V_{CB} is likely to be 0.9 V negative compared to the potential of the H$^+$/H$_2$ couple, indicating the sufficient potential for water reduction. On the other hand, the fact that V_{VB} is more than 0.6 V negative of the H$_2$O/O$_2$ couple rules out the possibility of overall water splitting on this electrode in a single-junction configuration.

Properties of modified CuInS$_2$ electrodes for H$_2$ evolution

Figures 5a and b show current–potential curves of the CuInS$_2$ electrode and that modified with Pt deposits (Pt–CuInS$_2$) in 0.1 mol L Na$_2$SO$_4$ solution with pH adjusted to 4, respectively. The bare CuInS$_2$ film showed little photoresponse, whereas the platinized CuInS$_2$ film exhibited appreciable increases in photocurrents, indicating the effectiveness of loading Pt deposits as promoters for H$_2$ production because of the low activity of the bare CuInS$_2$ surface for water reduction. The photocurrent onset potential of the Pt-CuInS$_2$ electrode was estimated to be −0.55 V (vs Ag/AgCl). This value is more negative than that of the onset potential of the above CuInS$_2$ system measured in a Eu^{3+} solution, even though the measurement was carried out at the same pH. These results suggest that there is a significant potential barrier or a large number of surface defects that hinder electron transfer to the surface-loaded Pt deposits.

To improve the photoresponse of the Pt-CuInS$_2$ electrode, n-type thin layers (ca. 100 nm) of CdS and ZnS were inserted by using chemical bath deposition (CBD) techniques, which are widely employed to fabricate p-n junctions for chalcopyrite-based solar cells.[11d, 17] Figures 5c and 5d show typical current–potential curves of these films (i.e., Pt–CdS/CuInS$_2$ and Pt–ZnS/CuInS$_2$) measured in an aqueous Na$_2$SO$_4$ solution with pH adjusted to 4. It is clear that insertion of n-type layers significantly improved cathodic photocurrents. Moreover, these modifications resulted in appreciable positive shifts of onset potentials of about 0–0.1 V vs Ag/AgCl, which is comparable to or slightly more positive than the onset potential observed in the above CuInS$_2$/Eu^{3+} system.

As reported previously, the series of chalcopyrite compounds can utilize the solid/liquid junction for charge separa-
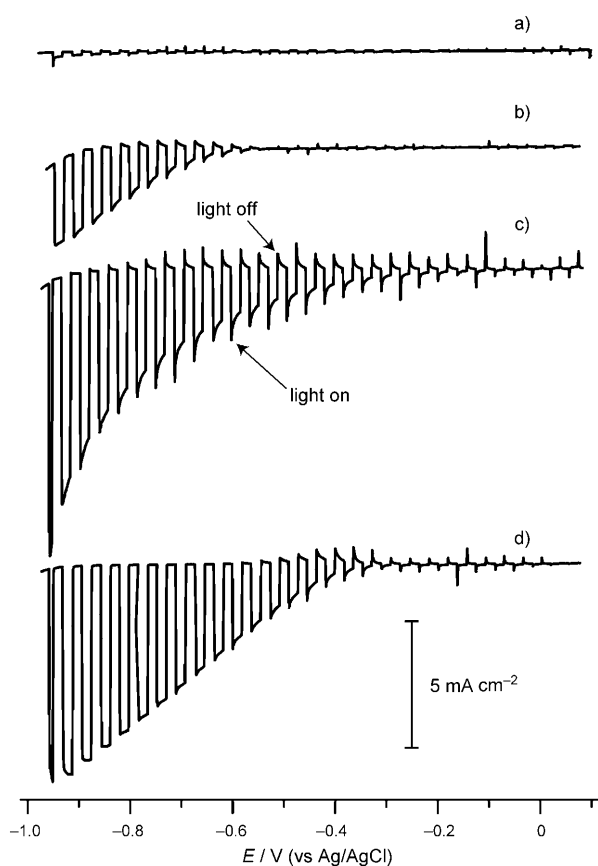
Figure 5. Current density vs potential scans of a) CuInS$_2$, b) Pt-CuInS$_2$, c) Pt-CdS/CuInS$_2$, and d) Pt-ZnS/CuInS$_2$ in Na$_2$SO$_4$ solution (0.1 mol L^{-1}) with pH adjusted to 4 under chopped illumination from a Xe lamp.

Figure 6. IPCE spectra of a) Pt-CdS/CuInS$_2$ and b) Pt-ZnS/CuInS$_2$ measured at −0.8 V vs Ag/AgCl in Na$_2$SO$_4$ solution (0.1 mol L) with pH adjusted to 4.

tion.[12] The present results indicate considerable facilitation of efficient charge separation by the introduction of *p*-n junctions, as has been proposed in a similar system based on the Cu(In,Ga)Se$_2$ (CIGS) thin film.[12f] The surface coverage of the n-type layers would also compensate surface defects of the CuInS$_2$ film to suppress interface recombination. Moreover, modulation of the electric structure of the solid/liquid interface should occur due to the surface modification. Although the exact mechanism is not known, such multiplication effects are likely to induce an efficient photocurrent for H$_2$ production.

Figure 6 shows the spectral responses of Pt-CdS/CuInS$_2$ and Pt-ZnS/CuInS$_2$ electrodes measured at −0.8 V vs Ag/AgCl in an aqueous Na$_2$SO$_4$ solution (pH 4). The IPCE spectrum of the Pt–CdS/CuInS$_2$ sample showed a rise at wavelengths ranging from 400 to 500 nm and it reached IPCE as high as 20% at wavelengths ranging from ca. 500 to 750 nm; the IPCE value declined steeply at wavelengths longer than 800 nm, which is almost in agreement with E_g, as determined above. The appearance of the rise of IPCE on the Pt–CdS/CuInS$_2$ sample at the short wavelength region suggests a filtering effect of the CdS ($E_g = 2.4$ eV) buffer to decrease effective photoabsortion at the CuInS$_2$ film (i.e., photons absorbed at the front n-type layer could not utilize H$_2$ liberation).[18] Compared to the Pt–CdS/CuInS$_2$ electrode, the spectrum of the Pt–ZnS/CuInS$_2$ electrode reaches IPCE in a maximum region (ca. 15%) even at
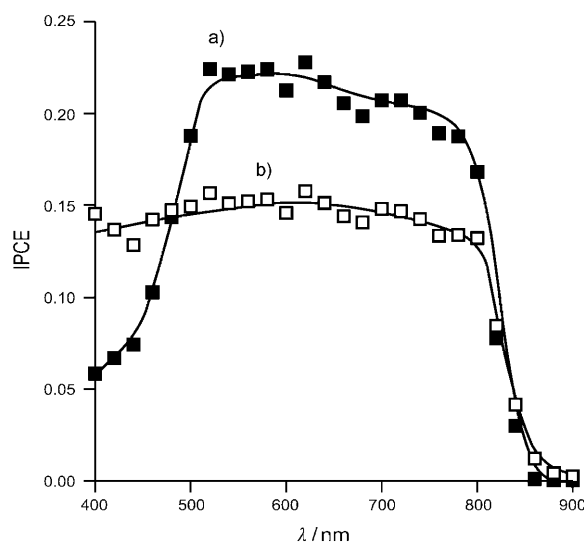
wavelengths shorter than 500 nm and maintains high IPCE values of up to 800 nm. This result suggests the advantage of the use of wide-gap n-type layer (e.g., $E_g = 3.6$ eV for ZnS) for the effective utilization of incident photons, though the absolute IPCE value of the present Pt–ZnS/CuInS$_2$ electrode in the maximum part is smaller than that of the P–CdS/CuInS$_2$ electrode. The lower IPCE of the Pt-ZnS/CuInS$_2$ electrode compared to that of Pt–CdS/CuInS$_2$ would be due to the difficulty associated with the ZnS deposition compared to that of the CdS layer.[11d, 17] Further studies are underway in our laboratory.

Figure 7 shows LSV plots of the Pt–CdS/CuInS$_2$ electrode in Na$_2$SO$_4$ solution (0.1 mol L^{-1}) with pH to 9 and 13. In contrast to the current–voltage curve in an acidic solution shown in Figure 5 c, results obtained in these basic solutions are comparable: there is almost no shift of the onset potentials (vs Ag/AgCl) regardless of the electrolyte solution pH. Due to these characteristics, the electrode becomes responsible for appreciable photocurrent generation in the "power-producing" region (i.e., > 0 V vs RHE).

It is generally believed that the barrier height in a metal-coated semiconductor electrode is solely dependent on the metal–semiconductor junction and is independent of the nature of the solution. Hence, the current onset should shift in the cathodic direction along with the RHE potential as the pH is increased. However, this is true only in the case where the layer covers the semiconductor surface continuously. It has been shown by Pt-Si[19] and Pt-CdS[20] interfaces that if the metal layer is discontinuous (i.e., if it consists of metal islands of fine particles), the energy diagram of the metal-modified semiconductor electrode/solution interface becomes comparable to that of the unmodified semiconductor electrode/solution interface. Namely, the flat band potential (V_{FB}) of the semiconductor is not altered by the modification of the metal particles. As V_{FB} of CdS is independent on solution pH (ca. −1.0 V, vs Ag/AgCl), there is also no pH dependence on the CdS electrode modified with such Pt fine particles. As shown in a typi-
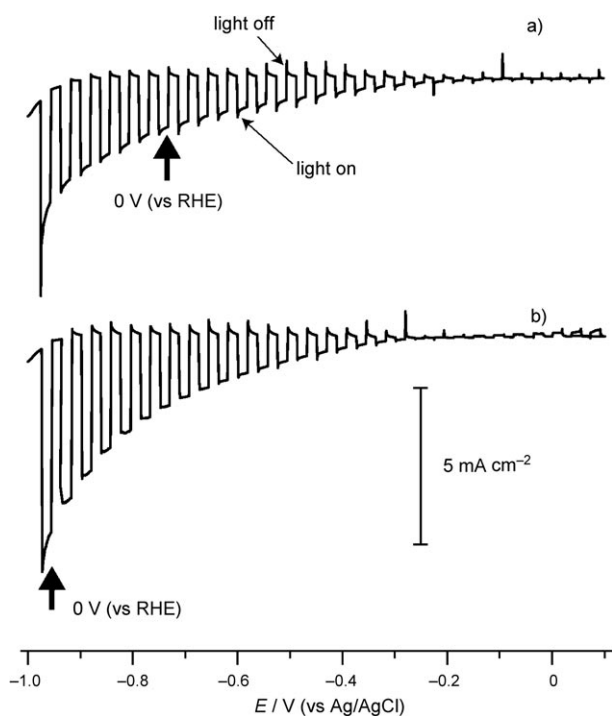
Figure 7. Current density vs potential scans of the Pt-CdS/CuInS$_2$ electrode in Na$_2$SO$_4$ solution (0.1 mol L^{-1}) with pH adjusted to a) 9 and b) 13 under chopped illumination from a Xe lamp.

cal SEM image of the present Pt-CdS/CuInS$_2$ electrode, surface Pt components formed island structures with particle sizes of several tens of nanometers (Figure 8). No pH dependence of current density-potential curves shown in Figure 7 is therefore attributed to this discontinuous distribution of Pt components.
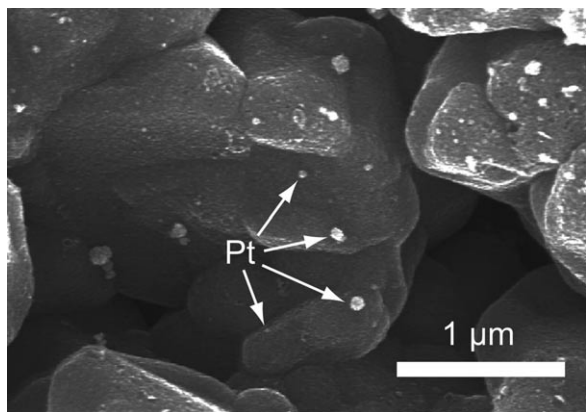

Figure 8. An SEM image of the Pt-CdS/CuInS$_2$ surface.

To confirm the H$_2$ liberation ability on a power generating region, the amount of H$_2$ evolved on the Pt-CdS/CuInS$_2$ electrode in Na$_2$SO$_4$ solution (0.1 mol L^{-1}, pH 13) with -0.8 V (vs Ag/AgCl) of applied bias was quantified. Figure 9 shows a typical time course curve of H$_2$ evolution. A time course curve of half amount of electrons passing through the outer circuit (e^-_{half}), which corresponds to the number of H$_2$ equivalents pre-
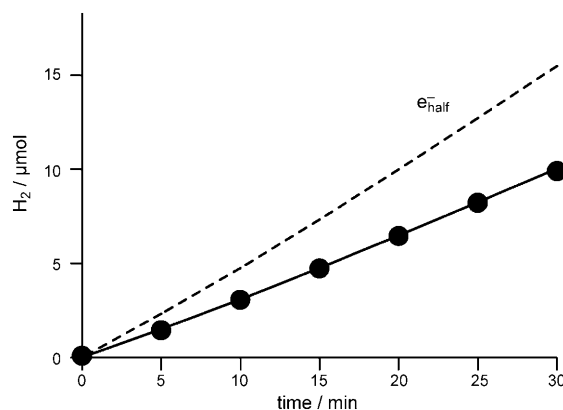

Figure 9. A time course curve of H$_2$ evolution on the Pt-CdS-CuInS$_2$ electrode in aqueous Na$_2$SO$_4$ solution (0.1 mol L^{-1}, pH 13) at -0.8 V (vs Ag/AgCl) under visible light irradiation from a Xe lamp. A dotted line denotes a time course curve of e^-_{half} during the H$_2$ evolution.

dicted assuming all electrons passing through the outer circuit go to make H$_2$, is also shown as a dotted line in this figure. It is clear from this figure that H$_2$ evolved continuously without any decrease in its rate, whereas the amount of H$_2$ evolved was less than the e^-_{half} line. Based on the thickness of the CuInS$_2$ film used (less than 1.5 μm; Figure 2 b) and the density of CuInS$_2$ (4.6 g cm^{-3}), the amount of CuInS$_2$ was estimated to be 2 μmol at most. The fact that the amount of H$_2$ evolved for 30 min photoirradiation (ca. 10 μmol) exceeded that of CuInS$_2$ demonstrates catalytic function of the electrode. As the system includes appreciable amounts of evolved O$_2$ at the Pt counter electrode and contaminated from the air, the smaller amounts of evolved H$_2$ than the e^-_{half} line is likely to be due to the formation of H$_2$O on the Pt deposits and Pt counter electrode. In addition, we also confirmed H$_2$ evolution even under a lower applied bias (e.g., -0.6 or -0.4 V (vs Ag/AgCl)), although the amounts of H$_2$ evolved were smaller than those under -0.8 V (data not shown).

As discussed in the above XRD analysis, the CuInS$_2$ layer prepared in the present study includes the Cu$_{11}$In$_9$ contaminant. The presence of this conductive component should generate shunt paths, leading to a decrease in induced IPCE (Figure 6). In addition, the presence of many crevices at the interface between the CuInS$_2$ layer and the Mo back contact shown in Figure 2 b seemed to generate a large series resistance, which is also unfavorable for efficient photon conversion into H$_2$. Therefore, by overcoming these problems associated with the CuInS$_2$ photoabsorber layer and by improving the *p*-n heterojunction (see above), present devices can be further improved.

Conclusions

A CuInS$_2$ film was fabricated on a Mo-coated glass substrate by the electrodeposition technique. Photoelectrochemical characterization clarified the flat band potential of the compound: this revealed the requirement of a bias potential or integration in a tandem device to induce overall water splitting on this material. The formation of heterojunctions by surface

coverage of the CuInS$_2$ film with n-type buffer layers, such as CdS and ZnS, followed by loading of Pt deposits made them efficient H$_2$-evolving photoelectrodes. For the CdS modified sample, IPCEs of more than 20% were achieved at wavelengths ranging from 500 to 750 nm by applying a potential at −0.8 V vs Ag/AgCl (pH 4). Moreover, quantitative analysis of H$_2$ production performed in alkaline solution (pH 13) under potentials of power-producing regions proved a sufficient catalytic function of the sample. Because the present CuInS$_2$ film still includes structural faults, further enhancement of conversion efficiency is expected by improvements in fabrication conditions of the CuInS$_2$ films. Improvements of fabrication conditions and materials to form the *p*-n junction are also required. Although the materials used in the present study include typical rare and/or toxic elements such as In, Cd, and Pt, our system can be extended to the electrodes based on mass abundant and less-toxic elements. Thus, studies along these lines are now in progress.

Experimental Section

A thin film of polycrystalline CuInS$_2$ was deposited by the electrodeposition technique.[21] On a molybdenum-coated soda lime glass (Mo/glass), metallic Cu and In layers were deposited successively under potentiostatic control using a Hokuto Denko HSV-100 potentiostat-galvanostat. Cu deposition was performed at −0.4 V (vs Ag/AgCl) in an aqueous solution containing CuSO$_4$ (10 mmol L^{-1}) and citric acid (10 mmol L^{-1}) with pH adjusted to 1.5. Deposition of the In layer on the Cu-covered Mo/glass was performed at −0.8 V (vs Ag/AgCl) in an aqueous 12 mol L^{-1} InCl$_3$ solution with pH adjusted to 2.2. The amount of each metal deposited was estimated by the electric charge: in the present study, electric charges of Cu and In depositions were fixed at 0.57 C cm^{-2} and 0.66 C cm^{-2}, respectively. Thus-obtained metallic precursor films were sulfurized under H$_2$S (5% in Ar) flow at 520 °C for 5 min. Before the electrochemical experiments, thus-obtained CuInS$_2$ films were etched by immersion in an aqueous KCN solution (10%) for 2 min to remove excess Cu$_x$S components. Crystallographic features of the CuInS$_2$ films before and after KCN treatment were evaluated by X-ray diffraction (XRD) using a Rigaku MiniFlex X-ray diffractometer (Cu Kα, Ni filter). The surface morphology and a cross section of the CuInS$_2$ film were observed using a Hitachi S-5000 FEG scanning electron microscope. Some of the CuInS$_2$ films were modified by coverage of a CdS or ZnS layer by chemical bath deposition (CBD) methods reported in the literature.[11d, 17]

Photoelectrochemical properties of bare CuInS$_2$ films were measured in an aqueous solution containing Eu(NO$_3$)$_3$ (50 mmol L^{-1}) as an electron scavenging electrolyte with pH adjusted to 4. A Pyrex electrolytic cell having a flat window was used. The photocurrent response of the film was measured under potentiostatic control using a three-electrode system with a Pt wire counter electrode and an Ag/AgCl reference electrode. Transient photocurrents were obtained by chopped illumination from a 300 W xenon lamp. The photocurrent spectrum was measured under N$_2$ using the lock-in technique. For this measurement, irradiation of the CuInS$_2$ film was performed by chopping at 10 Hz of monochromatic light, which was obtained by passing light from the 300 W Xe lamp through a monochromator. The number of incident photons was determined by an OPHIR Orion laser power meter equipped with a photodiode.

Photochemical H$_2$ production on CuInS$_2$ and on CuInS$_2$ modified with CdS and ZnS layers was carried out using the above photoelectrochemical setup. Prior to measurements, some of the electrode samples were photoirradiated in an N$_2$ saturated Na$_2$SO$_4$ solution (0.1 mol L^{-1}) containing H$_2$PtCl$_6$ (1 mmol L, pH adjusted to 4) at −0.1 V (vs Ag/AgCl) to load Pt deposits on their surfaces. For the H$_2$ liberation reaction, an aqueous Na$_2$SO$_4$ solution (0.1 mol L^{-1}) was employed as an electrolyte. Transient current–potential curves and photocurrent spectra of the samples were recorded by the same procedure as that used for the above-mentioned photoelectrochemical measurements of a bare CuInS$_2$ sample. Amount of evolved H$_2$ on a selected sample at fixed potentials was quantified by online gas chromatography using a Varian 490-GC-2010 gas chromatograph equipped with a MS-5 A column and a thermal conductivity detector (TCD) detector.

[1] A. J. Bard, M. A. Fox, *Acc. Chem. Res.* **1995**, *28*, 141–145.
[2] a) K. Domen, J. N. Kondo, M. Hara, T. Takata, *Bull. Chem. Soc. Jpn.* **2000**, *73*, 1307–1331; b) K. Maeda, K. Domen, *J. Phys. Chem. C* **2007**, *111*, 7851–7861; c) F. E. Osterloh, *Chem. Mater.* **2008**, *20*, 35–54; d) A. Kudo, Y. Miseki, *Chem. Soc. Rev.* **2009**, *38*, 253–278.
[3] a) Y. Inoue, T. Kubokawa, K. Sato, *J. Chem. Soc. Chem. Commun.* **1990**, 1298–1299; b) T. Takata, Y. Furumi, K. Shinohara, A. Tanaka, M. Hara, J. N. Kondo, K. Domen, *Chem. Mater.* **1997**, *9*, 1063–1064; c) S. Ikeda, M. Hara, J. N. Kondo, K. Domen, H. Takahashi, T. Okubo, M. Kakihana, *Chem. Mater.* **1998**, *10*, 72–77; d) J. Sato, N. Saito, H. Nishiyama, Y. Inoue, *J. Phys. Chem. B* **2001**, *105*, 6061–6063; e) H. Kato, K. Asakura, A. Kudo, *J. Am. Chem. Soc.* **2003**, *125*, 3082–3089; f) S. Ikeda, T. Itani, K. Nango, M. Matsumura, *Catal. Lett.* **2004**, *98*, 229–233; g) T. Hisatomi, K. Miyazaki, K. Takanabe, K. Maeda, J. Kubota, Y. Sakata, K. Domen, *Chem. Phys. Lett.* **2010**, *486*, 144–146.
[4] J. Sato, N. Saito, Y. Yamada, K. Maeda, T. Takata, J. N. Kondo, M. Hara, H. Kobayashi, K. Domen, Y. Inoue, *J. Am. Chem. Soc.* **2005**, *127*, 4150–4151.
[5] K. Maeda, K. Teramura, D. Lu, T. Takata, N. Saito, Y. Inoue, K. Domen, *Nature* **2006**, *440*, 295.
[6] A. Fujishima, K. Honda, *Nature* **1972**, *238*, 37–38.
[7] T. Bak, J. Nowotny, M. Rekas, C. C. Sorrell, *Int. J. Hydrogen Energy* **2002**, *27*, 991–1022.
[8] a) E. L. Miller, B. Marsen, D. Paluselli, R. Rocheleau, *Electrochem. Solid-State Lett.* **2005**, *8*, A247 A249; b) S. Yamane, N. Kato, S. Kojima, A. Imanishi, S. Ogawa, N. Yoshida, S. Nonomura, Y. Nakato, *J. Phys. Chem. C* **2009**, *113*, 14575–14581.
[9] a) O. Khaselev, J. A. Turner, *Science* **1998**, *280*, 425–427; S. Licht, B. Wang, S. Mukerji, T. Soga, M. Umeno, H. Tributsch, *J. Phys. Chem. B* **2000**, *104*, 8920–8924.
[10] a) H. Wang, T. Lindgren, J. He, A. Hagfeldt, S.-E. Lindquist, *J. Phys. Chem. B* **2000**, *104*, 5686–5696; b) J. H. Park, A. J. Bard, *Electrochem. Solid-State Lett.* **2006**, *9*, E5–E8; c) A. Wolcott, W. A. Smith, T. R. Kuykendall, Y. Zhao, J. Z. Zhang, *Adv. Funct. Mater.* **2009**, *19*, 1849–1856; d) W. J. Youngblood, S.-H. A. Lee, K. Maeda, T. E. Mallouk, *Acc. Chem. Res.* **2009**, *42*, 1966–1973.
[11] a) J. Klaer, J. Bruns, R. Henninger, K. Siemer, R. Klenk, K. Ellmer, D Bräunig, *Semicond. Sci. Technol.* **1998**, *13*, 1456–1458; b) H.-W. Schock, R.

Noufi, *Prog. Photovolt. Res. Appl.* **2000**, *8*, 151–160; c) K. Siemer, J. Klaer, I. Luck, J. Bruns, R. Klenk, D. Braunig, *Sol. Energy Mater. Sol. Cells* **2001**, *67*, 159–166; d) A. Ennaoui, M. Bär, J. Klaer, T. Kropp, R. Sáez-Araoz, M. C. Lux-Steiner, *Prog. Photovolt. Res. Appl.* **2006**, *14*, 499–511; e) I. Repins, M. Contreras, B. Egaas, C. De Hart, J. Scharf, C. L. Perkins, B. To, R. Noufi, *Prog. Photovolt. Res. Appl.* **2008**, *16*, 235–239.

[12] a) A. Kisilev, V. Marcu, D. Cahen, H. W. Schock, R. Noufi, *Sol. Cells* **1990**, *28*, 57–67; b) J. Kessler, D. Lincot, J. Vedel, B. Dimmler, H. W. Schock, *Sol. Cells* **1990**, *29*, 267–281; c) A. M. Fernández, N. Dheree, J. A. Turner, A. M. Martínez, L. G. Arriaga, U. Cano, *Sol. Energy Mater. Sol. Cells* **2005**, *85*, 251–259; d) R. C. Valderrama, P. J. Sebastian, J. P. Enriquez, S. A. Gamboa, *Sol. Energy Mater. Sol. Cells* **2005**, *88*, 145–155; e) B. Marsen, B. Cole, E. L. Miller, *Sol. Energy Mater. Sol. Cells* **2008**, *92*, 1054–1058; f) D. Yokoyama, T. Minegishi, K. Maeda, M. Katayama, J. Kubota, A. Yamada, M. Konagai, K. Domen, *Electrochem. Commun.* **2010**, *12*, 851–853.

[13] a) T. Todorov, E. Cordoncillo, J. F. Sanchez-Royo, J. Carda, P. Escribano, *Chem. Mater.* **2006**, *18*, 3145–3150; b) V. Izquierdo-Roca, A. Pérez-Rodríguez, J. R. Morante, J. Álvarez-García, L. Calvo-Barrio, V. Bermudez, P. P. Grand, L. Parissi, C. Broussillon, O. Kerrec, *J. Appl. Phys.* **2008**, *103*, 123109.

[14] S. Jost, R. Schurr, A. Hölzing, F. Hergert, R. Hock, M. Purwins, J. Palm, *Thin Solid Films* **2009**, *517*, 2136–2139.

[15] a) M. A. Butler, *J. Appl. Phys.* **1977**, *48*, 1914–1920; b) T. Torimoto, S. Takabayashi, H. Mori, S. Kuwabata, *J. Electroanal. Chem.* **2002**, *522*, 33–39.

[16] M. I. Alonso, K. Wakita, J. Pascual, M. Garriga, N. Yamamoto, *Phys. Rev. B* **2001**, *63*, 075203.

[17] S. Ikeda, R. Kamai, T. Yagi, M. Matsumura, *J. Electrochem. Soc.* **2010**, *157*, B99-B103.

[18] R. Scheer, T. Walter, H. W. Schock, M. L. Fearheiley, H. J. Lewerenz, *Appl. Phys. Lett.* **1993**, *63*, 3294–3296.

[19] a) Y. Nakato, H. Tsubomura, *J. Photochem.* **1985**, *29*, 257–266; b) Y. Nakato, H. Tsubomura, *Electrochim. Acta* **1992**, *37*, 897–907.

[20] M. Matsumura, T. Uchihara, K. Hanafusa, H. Tsubomura, *J. Electrochem. Soc.* **1989**, *136*, 1704–1709.

[21] a) J. Herrero, J. Ortega, *Sol. Energy Mater.* **1990**, *20*, 53–65; b) S. Nakamura, A. Yamamoto, *Sol. Energy Mater. Sol. Cells* **2003**, *75*, 81–86; c) D. Lincot, J. F. Guillemoles, S. Taunier, D. Guimard, J. Sicx-Kurdi, A. Chaumont, O. Roussel, O. Ramdani, C. Hubert, J. P. Fauvarque, N. Bodereau, L. Parissi, P. Panheleux, P. Fanouillere, N. Naghavi, P. P. Grand, M. Benfarah, P. Mogensen, O. Kerrec, *Sol. Energy* **2004**, *77*, 725–737.